NASA TM-87668

NASA Technical Memorandum 87668

A MODEL FOR THE KINETICS OF A SOLAR-PUMPED LONG PATH LASER EXPERIMENT

L. V. Stock, J. W. Wilson, and R. J. De Young

May 1986

NASA
National Aeronautics and Space Administration

Langley Research Center
Hampton, Virginia 23665

ABSTRACT

A kinetic model for a solar-simulator-pumped iodine laser system is developed and compared to an experiment in which the solar simulator output is dispersed over a large active volume (150 cm^3) with low simulator light intensity (≈200 solar constants). A trace foreign gas which quenches the upper level is introduced into the model to simulate the foreign gas introduced upon filling. Furthermore, a constant representing optical absorption of the stimulated emission is introduced, in addition to a constant representing the scattering at each of the mirrors, via the optical cavity time constant. The non-uniform heating of the gas is treated as well as the pressure change as a function of time within the cavity. With these new phenomena introduced into the kinetic model, a best reasonable fit to the experimental data is found by adjusting the reaction-rate coefficients within the range of known uncertainty by numerical methods giving a new bound within this range of uncertainty. The experimental parameters modeled are the lasing time, laser pulse energy, and time-to-laser threshold.

This Page Intentionally Left Blank

TABLE OF CONTENTS

INTRODUCTION

Direct conversion of solar radiation into laser energy via a population inversion can be applied to space power transmission and spacecraft propulsion. Alkyl iodide gases have been shown to be good candidates for solar pumping in solar-simulator demonstrations (ref. 1). For space power applications, the solar-pumped alkyl iodide gas laser has to be scaled to encompass large space systems. In order to accomplish this task, the reaction rate coefficients for alkyl iodide gas chemical kinetics need to be defined.

A kinetic model of a solar-simulator-pumped iodine laser is being developed to obtain the reaction rate coefficients of the alkyl iodide gas laser. Prior to this experiment which uses $i\text{-}C_3F_7I$ as the lasant, the simulator experiments were marked by a high solar concentration (≈10,000 solar constants) and a small active volume (3 - 4 cm^3) (refs. 1 and 2). In those studies, the laser threshold was dominated by the loss of the upper laser level through recombination and quenching (ref. 2). After threshold is achieved, the formation of I_2 is the dominate reaction which determines how long the system will lase since I_2 is a strong quencher of the upper laser level. Because of the high solar concentration in these prior experiments, the I_2 buildup rate was sufficiently rapid that the laser was effectively quenched after about 3 milliseconds (ref. 1). Thus, such a system would make continuous-wave operation extremely difficult.

A new experimental system is presented here in which the solar simulator output is dispersed over a relatively large active volume (150 cm^3), and a greatly reduced simulator light intensity (≈200 solar

constants) is used. With this new experimental arrangement, the kinetic model is tested under vastly different operating conditions than that of prior experiments. Herein, information about the kinetic characteristics not accessible in earlier experiments is revealed. With this new experimental approach, some changes are introduced into the kinetic model. A trace foreign gas which quenches the upper laser level is introduced into the system upon filling. A constant, representing absorption of the stimulated emission, is introduced via an optical cavity time constant (ref. 1). The non-uniform heating of the gas is treated as well as the pressure change as a function of time within the cavity. With these new phenomena introduced into the kinetic model, a best reasonable fit to the experimental data is found by adjusting the reaction rate coefficients within the range of known uncertainty by numerical methods. Depending on the physical characteristics of the output parameters, the chemical reaction rates found within this range represent a new upper or lower bound.

SOLAR SIMULATOR SETUP

The present experimental setup has two light sources consisting of xenon arc discharges across 8-mm gaps that are stabilized by a 1030-kPa (10.2 atm) Xe-flow. The light of the arc lamps is reflected from high quality elliptic aluminum reflectors and focused near the shutter planes as shown in figure 1. The reflectors have a vapor deposited MgF_2 coating to prevent surface oxydation and abrasion. The broad spectral content of the arc plasma corresponds to black body emission at approximately 6000 K. The energy content of the UV light is approximately twice that of a 6000 K

blackbody at the focus of each reflector. The divergent light beam leaving each focus is adjusted to intersect a flat plate laser cell in which the lasing gas is contained. The transparent cell walls are constructed of 6-mm thick UV enhanced fused silica plates.

In figure 2 the geometry of the laser cavity is shown with its associated area of solar simulator light impinging on the laser path. The solar simulator radiation pattern is in the shape of a doughnut and in figure 2 is the volume of excitation given by V. The laser cavity is a box with turning mirrors of maximum reflectivity at 1.3 μm at three of the corners to direct the coherent light through the most intense region of the solar simulator light. At the fourth corner there are two Brewster windows, a back mirror (maximum reflectivity at 1.3 μm), and a variable output mirror such that the path length is twice through the resonator cavity.

The light intensity in the volume of excitation was measured with a calorimeter, and the integral of the light intensity over the optical center line of the resonator cavity was calculated for each of the two lamps. Since the light intensity is relatively uniform in the volume of the resonator cavity, we assume a constant photodissociation rate averaged over the optical center line within the gas filled laser cell. The average solar concentration at the laser cell centerline was found to be 150 solar constants (1 solar constant = 1.353 kW/m^2) over a 61.5 cm pathlength for the simulators operating at 400 amps each. The photodissociation rate is given by the integral over the photodissociation cross section and the blackbody photon flux. Results for a 6000 K blackbody is (ref. 1 and 2)

$$\xi(\vec{x}) = T_t \, S \, n \, [f \exp(-n\sigma_0 x) + (1-f) \exp(-.223 n\sigma_0 x)] \, C(\vec{x}) \qquad (1)$$

where S (maximum photodissociation rate) , σ_0 (absorption cross section), and f (the fractional absorption near the line center) are given in table $\vec{I}$. C(x) is the local light intensity in units of solar constants. The alkyl iodide photodissociation rates are doubled in the model to account for the excess UV in the laboratory light source. The transmission coefficient for the 6-mm fused silica plates, T_t, is on the order of 0.96, x is the slant distance through the gas in reaching the point $\vec{x}$, and n is the alkyl iodide gas density.

PHOTOLYSIS OF THE ALKYL IODIDES

The chemical and physical processes of illumination of the alkyl iodides has been discussed elsewhere (refs. 1, 2, and 3). The major kinetic pathways from the photodissociation of alkyl iodide are shown in figure 3. Previous studies (refs. 1 and 2) have shown that the laser threshold is dominated by the processes

$$R + I^* \xrightarrow{K_1} RI$$

which limits the amount of inversion achievable for a given light intensity, and

$$RI + I^* \xrightarrow{Q_1} I + RI$$

which reduces the inversion intensity by loss of the upper level (ref. 2). As the kinetics of the system continues, there is a slow buildup of I_2 which is a strong quencher of the upper laser level. The formation of I_2 is in competition with

$$R + I \xrightarrow{K_2} RI$$

and occurs through

$$I + I + RI \xrightarrow{C_2} I_2 + RI$$

which is a three-body recombination reaction.

A model of the photodissociation and subsequent chemical reactions have been derived previously (refs. 1, 2, and 3) and are given with modifications described later, as

$$\frac{d[RI]}{dt} = K_1 [R] [I^*] + K_2 [R] [I] - \varepsilon_1[RI] - K_4[R] [RI] \tag{2}$$

$$\frac{d[R]}{dt} = \varepsilon_1 [RI] - K_1[R] [I^*] - K_2[R][I] - 2K_3[R]^2 - K_4 [R][RI] \tag{3}$$

$$\frac{d[R_2]}{dt} = K_3[R]^2 + K_4 [R][RI] \tag{4}$$

$$\begin{aligned}\frac{d[I_2]}{dt} &= C_1 [I] [I^*] [RI] + C_2 [I]^2[RI] + C_3[I][I^*][I_2] \\ &\quad + C_4[I]^2[I_2] - \varepsilon_2[I_2]\end{aligned} \tag{5}$$

$$\begin{aligned}\frac{d[I^*]}{dt} &= \varepsilon_1[RI] + \varepsilon_2[I_2] - K_1[R][I^*] - C_1[I][I^*][RI] \\ &\quad - C_3[I][I^*][I_2] - Q_1[I^*][RI] - Q_2[I^*][I_2] \\ &\quad - r_{max} - A[I^*] - \frac{[I^*]}{\tau_D} - Q_{FG}[FG][I^*]\end{aligned} \tag{6}$$

$$\begin{aligned}\frac{d[I]}{dt} &= \varepsilon_2[I_2] + Q_1[I^*][RI] + Q_2[I^*][I_2] + r_{max} - A[I^*] \\ &\quad - C_1[I][I^*][RI] - 2C_2[I]^2 [RI] - C_3[I][I^*][I_2] \\ &\quad - 2C_4[I]^2[I_2] - K_2[R][I] - \frac{[I]}{\tau_D} + Q_{FG}[FG][I^*] \\ &\quad + K_4 [R][RI]\end{aligned} \tag{7}$$

where [FG] is the foreign gas density, L is the lamp image length parameter, L_c is the distance between laser cavity mirrors, ξ_i is the photodissociation rate of the associated chemical species, and τ_D is the diffusion time constant. In addition, the rate of change of the photon density ρ is given by

$$\frac{d\rho}{dt} = r_{max} \frac{L}{L_c} - \frac{1}{\tau_c} \rho + gA[I^*] \tag{8}$$

where τ_c is the optical cavity time constant, g is the coupling parameter of the spontaneous emission to the optical cavity (ref. 1), and A the Einstein coefficient. The stimulated emission rate is given by

$$r_{max} = c\sigma\rho \left([I^*] - \frac{1}{2}[I]\right) \tag{9}$$

where σ is the stimulated emission cross section discussed later. The kinetic rate coefficients for the propyl iodides were compiled elsewhere (ref. 2) and are given in table II. The laser kinetics are described through equations (8) and (9) along with the corresponding coupling terms through the stimulated emission rate in equations (6) and (7). The diffusion time constant may be evaluated from the point diffusion model as we did before (ref. 2) and for a flat plate arrangement,

$$n_{I^*}(0,t) = n_0 \, \mathrm{erf}(r_0/\sqrt{(4Dt)}) \tag{10}$$

The diffusion time constant is

$$\tau_D \approx 9 \, r_0^2/4D \tag{11}$$

where r_0 is the halfwidth of the laser cell and D is the diffusion constant ($D \approx 73$ cm^2 - torr/sec from ref. 2).

Furthermore, because of the flat plate arrangement (fig. 2) the optical cavity time constant τ_c is now given as

$$\tau_c = \frac{-2(L_c/c)}{\ln(r_1^7 r_2^4 r_3 \tau_s^{10})} \tag{12}$$

where r_1 is the reflection coefficient (0.9975) at the corners of the cavity, r_2 is the Brewster window loss (0.98), r_3 is the output mirror reflectivity and τ_s is a parameter introduced to account for the loss because of scattering from a possible film formed on each of the internal mirrorsurfaces. The optical cavity time constant is modified as α_{loss} changes and is given as

$$\tau_c' = \frac{\tau_c}{(1 + c\alpha_{loss}\tau_c L/L_c)} \tag{13}$$

where α_{loss} is a parameter describing optical losses within the laser medium.

To find the output parameters of the kinetic model a quasi steady-state solution can be assumed, where the photon density becomes steady as gains and losses balance each other in the cavity and gain medium (ref. 1). With this assumption the derivative in equation (8) is equal to zero and

$$\rho = \Gamma_{max}\, \tau_c\, L/L_c \tag{14}$$

or after substitution of equation (9)

$$I_{th} \equiv [I^*] - \tfrac{1}{2}[I] = L_c/(L\, \tau_c\, c\, \sigma) \tag{15}$$

where I_{th} is the inversion density. Furthermore, from equation (6) under quasi steady-state conditions (ref. 1)

$$r_{max} = \varepsilon_1[RI] + \varepsilon_2|I_2| - K_1|R|[I^*] - Q_1[RI][I^*] - Q_2[I_2][I^*] \tag{16}$$

and the laser output power density (W/cm^2) is given by

$$P = \varepsilon_\nu \rho(1 - r_3) \tag{17}$$

where ε_ν is the photon energy and $(1 - r_3)$ is the output mirror transmission.

The maximum gain occurs for the transition from the F = 3 to the F = 4 quantum level in an iodine laser (ref. 2). The gain on this transition is given as

$$G_{34} = \sigma_{34}^* \{[I^*] - \tfrac{1}{2}[I]\} \tag{18}$$

and as a practical matter we take the stimulated emission cross section to be

$$\sigma_{34}^* = \frac{g_3}{g_2 + g_3} \sum_{FF'} \sigma_{FF'}(\nu_{34}) \tag{19}$$

as suggested by Fuss and Hola (ref. 4) which is strictly true only when collisional equilibrium is established among the hyperfine levels. Where g_2 and g_3 are the degeneracy of the hyperfine levels of the upper laser state and ν_{34} is the central frequency. The individual stimulated emission cross sections $\sigma_{FF'}(\nu)$ are functions of the line broadening

$$\Delta\nu = \alpha_0 + \alpha_1 P_o \tag{20}$$

where α_0 is related to the Doppler linewidth

$$\alpha_0 = 251 \sqrt{(T/T_0)} \quad (MHz) \tag{21}$$

and α_1 is the pressure broadening coefficient taking on the value

$$\alpha_1 = 14.8 \pm 4 \quad \text{(MHz/torr)} \tag{22}$$

at room temperature (ref. 2). The stimulated emission cross sections are then

$$\sigma_{FF'}(\nu) \approx \frac{\lambda^2 A_{FF'}}{8\pi} \; g_{FF'}(\nu) \tag{23}$$

where $g_{FF'}(\nu)$ is the corresponding line shape and $A_{FF'}$ is the transition rate.

Because of the long operation times of this laser system, there is a concern that sufficient energy is deposited in the gas to raise its temperature by hundreds of degrees. Therefore, heat transport in the gas is a prime consideration. A simple model of heat diffusion from the volume of exposed gas to the cooler gas and the cell walls is now derived which is used in the model.

The heat diffusion equation is given as

$$k\Delta^2 T(x) + q = \rho_g C_v \frac{dT(x)}{dt} \tag{24}$$

where k is the thermal conductivity, q the source of heat from photolysis, and $\rho_g C_v$ the heat capacity per unit volume. Considering the steady state solution for constant heating in slab geometry, the initial gas temperature is equal to the wall temperature T_w. The steady state gas temperature is given by

$$T(x) = \frac{1}{2} \; \frac{q}{k} \; (2r_0 - x)x + T_w \tag{25}$$

as a function of the cavity thickness. In addition, the heat diffusion can be approximated by

$$\rho_g C_v \frac{\partial T_m}{\partial t} = \frac{k}{2r_o} \left[(\nabla T)_{s_1} + (\Delta T)_{s_2} \right] + \bar{q} \tag{26}$$

where T_m is the midpoint gas temperature, $\bar{q}$ is the heat gained at the midpoint, and $(\nabla T)_s$ is the temperature gradient at the sides. An effective convection coefficient can be found from the steady state solution by

$$h(T_w - T_m) = \frac{k}{2r_o} \left[(\nabla T)_{s_1} + (\Delta T)_{s_2} \right] \tag{27}$$

which equals -q, and from equation (25)

$$T_m = T_w + \frac{r_o^2}{2} \frac{q}{k} \tag{28}$$

giving

$$h = \frac{2k}{r_o^2} \tag{29}$$

Therefore, using this value in the equation 26, the heat diffusion equation becomes

$$\rho_g C_v \frac{\partial T_m}{\partial t} = \frac{2k}{r_o^2} (T_w - T_m) + \bar{q} \tag{30}$$

which implies a relaxation time given as

$$\tau = r_o^2 \rho_g C_v / 2k \tag{31}$$

If k is taken to be

$$k = C_v \bar{v} / (4\pi N_o d^2) \tag{32}$$

where the heat capacity at constant volume C_v is about 40 cal/mol°C, $\bar{v}$ is the mean thermal speed of the diffusing particle, d is the distance traveled in thermalization, and ρ_g is the number of moles per unit volume (ref. 2); the relaxation time constant can be simplified as

$$\tau = 4\,\tau_D/9 \tag{33}$$

which can be used to model the midpoint gas temperature as a function of time.

A two region model is assumed, as shown in figure 2. The temperature differential for the lasant medium directly exposed by the simulator light is given by

$$\frac{dT_1}{dt} = q/\rho_g C_v - (T_1 - T_w)/\tau - (T_1 - T_2)/\tau \tag{34}$$

and for the unexposed medium close to the wall

$$\frac{dT_2}{dt} = (T_1 - T_2)/\tau - 1.5(T_2 - T_w)/\tau \tag{35}$$

where τ is a relaxation time given above for conduction to the wall and heat exchange between the two regions, and 1.5 is added to approximate the effect of the corners. The rate of internal heat generation of the system is approximated here as

$$q = \Delta E/\Delta V \Delta t \tag{36}$$

where ΔV and Δt are increments of volume and time, and the change in internal energy is given by

$$\Delta E = \varepsilon_0 S_1 dt + \varepsilon_1 K_1 [I^*][R]\,dt + \varepsilon_2 K_2 [I][R]\,dt + \varepsilon_3 K_3 [R][R]\,dt \tag{37}$$

where ε_i is the energy released to the medium due to the associated reactions (ref. 2).

The temperature change of the lasant is related to the change in internal energy of the gas and results in a fractional reduction in density

in the heated region of the cavity ρ'/ρ_o, where ρ_o is the initial density and ρ' is a function of time. Initially, the total volume of the cavity can be given as

$$V_t = V_o + V + V_1 \tag{38}$$

where V is the region directly influenced by the pulse energy (fig. 2), and V_1 and V_o are regions interior and exterior to V. The pressures and temperatures of the regions interior and exterior to the laser pulse are assumed to be identical. Therefore, the effective temperature of the cavity is given as

$$T_{eff} = \frac{V}{V_t} T_1 + \frac{V_o + V_1}{V_t} T_2 \tag{39}$$

since the energy in the cavity is conserved. In addition, the effective temperature of the cavity is given by

$$T_{eff} = \frac{V_1}{V_i'} T_W = \frac{V_o}{V_o'} T_W \tag{40}$$

where the prime indicates an intermediate state. Using the relationship

$$V' = V_t - V_i' - V_o' \tag{41}$$

in equation (40), then

$$\frac{V'}{V} = 1 + \frac{V_o - V_1}{V} \left(1 - \frac{T_W}{T_{eff}}\right) \tag{42}$$

which is also by definition the fractional reduction in density. After the use of equations (39) and (40), this fraction can now be written as

$$\rho' = \frac{\rho_o \, V/(V_o+V_1)}{V/(V_o+V_1) + [(1-T_1/T_2)/(1+T_1/T_2)]} \tag{43}$$

and this relationship is used to describe the change in pressure as a function of lasing time by using the previously derived relationships for T_1 and T_2.

RESULTS

To develop the model further, a reasonable fit to the data must be found via an adjustment of the rate coefficients, the foreign gas partial pressure introduced into the system, and the change in the optical cavity time constant describing the loss from the optical absorption along the laser path. This is done by varying these unknown parameters until a reasonable fit to the experimental data is found for different fill pressures and output mirror reflectivities (ref. 5). This search is done while considering the constraints of the error bounds defined in table II for the rate coefficients, along with a definition for reasonable output parameters when compared to the experimental data. The results of the search are given in table III. In addition, the foreign gas density [FG] is found to be 2.292×10^{12} cm^{-3}, and the parameter α_{loss} introduced in the optical cavity time constant τ_c is given as

$$\alpha_{loss} = 2.77765 \times 10^{-4} + (1.354 \times 10^{-7})\ P_0 \tag{44}$$

where P_0 is the fill pressure in torr. Furthermore, the optical scattering parameter τ_s introduced in the optical cavity time constant τ_c is found to be 0.995. The parameters found from the search are used to find the fit shown in figures 4, 5, and 6 for the lasing times, threshold times, and pulse energies, respectively.

The experimental results for the i-C_3F_7I laser are compared with the theory's prediction in figures 4, 5, and 6. In figure 4 the lasing time is plotted as a function of pressure; at high pressures the differences between the predicted values and the experimental data are smaller than at low pressures. This indicates that further physical phenomena need to

be added to the model, for example convection. The approach taken in the present analysis is that the experimental lasing time provides a lower bound to lasing time allowed by the gas chemistry. The experimental lasing time is determined by physical processes that are not in the model. As indicated in figure 4, the chemistry does not limit long-term lasing but probably convective motion, which would not be present in space operation. Convective motion is a probable candidate since it would reduce the amount of excited iodine available for stimulated emission. Figure 5 shows the experimental and theoretical results of the time to laser threshold. Except at low pressure, there is fair agreement with the experimental data (30 percent difference for the 85 percent output mirror at 11 torr). This is the result of the addition of a large amount of loss from unknown mechanisms (possibly aerosols) along the lasing path in the cavity model. Since the lasing times predicted by the model differ from the experimental lasing times, the pulse energy calculation is stopped at the time given experimentally. Thus, the pulse energy presented by the kinetic model is more indicative of an average power found soon after threshold. The results of this calculation are given in figure 6 as pulse energy relative to the fill pressures. A comparison is made with the experimental results, and general trends of the experimental data are expressed in the pulse energy calculations given by the model. For instance, in figure 6 there is a peak at 6 torr for both the theoretical prediction and the experimental data for the 85 percent output mirror.

Since the inversion density depends mainly on the kinetic coefficients K_1 and Q_1 and the diffusion coefficients (ref. 2), the lasing threshold is primarily determined by these coefficients. In addition, a term α_{loss}

describing the losses in the optical path is added into the calculation which affects the threshold times for the different experimental laser configurations. For the individual reactions the following are descriptions of how the pulse energies and lasing times are modified.

K_2 $R + I \rightarrow RI$

If the value of K_2 is increased, a larger number of parent molecules are produced after photodissociation and the formation of I_2 is prevented. Therefore, the lasing times and the pulse energy would decrease.

C_2 $I + I + RI \rightarrow I_2 + RI$

Increase the value of C_2, and the number of I_2 molecules is increased. This mechanism gives shorter lasing times and less energy output, since I_2 is a major quencher. In addition, fewer iodine atoms are available for recombination to the parent molecule RI.

K_1 $I^* + R \rightarrow RI$

If K_1 is increased, there are fewer excited iodine atoms to contribute to the pulse energy, thereby, reducing the power output and, as stated above, increasing threshold times.

Q_1 $I^* + RI \rightarrow RI + I$

If Q_1 is increased, the lasing times and pulse energies are reduced and the time to threshold is increased. This is because there are fewer excited iodine atoms.

Q_2 $I^* + I_2 \rightarrow I + I_2$

If Q_2 is increased, the lasing time is shortened, since the population density of the metastable state is reduced. Furthermore, Q_2 is taken as the reaction rate for the unknown filling gas, since it involves a quenching mechanism similar to the quenching mechanism of the unknown impurity, further reducing the population density.

The remaining reactions are of lesser importance in the kinetic model. By increasing the value of K_3 in the model, there are fewer radicals to recombine to form the parent gas RI. Therefore, the energy output is decreased. I_2 is a major quencher; therefore, if C_1 and C_3 are increased, energy outputs and lasing times decrease. The reactions governed by K_4 and C_4 do not affect the reaction until late laser times (later than presently considered).

In table II the experimental bounds as found in the literature are given for each of the rate coefficients. As stated earlier, these represent upper and a lower bounds to rates published earlier. The fit by numerical methods to the data found in the experiment described here gives a further bound for the rate coefficients. The physical constraints of the fit, in addition to how a change in the rate coefficients modifies the output parameter, determines whether the rate coefficient found by fitting the data is an upper or lower bound. In figure 5 the threshold times predicted by the kinetic model are longer than that which is demonstrated experimentally. Therefore, the kinetic reaction rates predicted by the model describe an upper bound. In addition, the model's lasing times given in figure 4 show only the chemical kinetic limits, therefore, a lower bound to these limits are indicated.

For a late time pulse, the quenching rate depends directly upon Q_2 and C_2 and inversely upon K_2 (ref. 1). Since the actual quenching rate can be

less than the quenching rate found, and the lasing times given by the kinetic model in figure 4 depend upon this rate, Q_2, C_2, and K_2 found by the fit represent upper and lower bounds. As stated previously, the kinetic coefficients of primary importance in determining the time to threshold are K_1 and Q_1 (ref. 2), since the inversion density depends on [I*] (eqn. 6). Therefore, the rate coefficients used to calculate the fit in figure 5 represent an upper bound for K_1 and Q_1. Finally, the laser output power density depends on the photodissociation rate and not on kinetic rate coefficients (ref. 1). Since the calculation of the pulse energies by the kinetic model shown in figure 6 is terminated at the lasing times given experimentally, the fit shown does not depend on the rate coefficients which determine the lasing times. Therefore, the fit by the kinetic model for the pulse power data does not determine a bound on the coefficients. These results are summarized in table IV giving the previously published bounds (ref. 2) compared to the bounds resulting from the fit by the kinetic model to the experimental data given in figures 4, 5, and 6. Tabulated are the rate coefficients which take a major role in determining this fit.

CONCLUDING REMARKS

A best fit to the experimental data is found for the computer model presented here. Within the context of the best fit, the upper and lower bounds of the experimental values of the rate constants are maintained. The rate constants are used to calculate the results for the lasing times, threshold times, and pulse energy which represent a physically reasonable fit. The fit implies that the chemistry which is modeled here is not the main limit on laser operation, but rather the laser is limited by physical

processes not in the present kinetic model. Hence, the model provides some bounds on the chemical reaction rates. Trends are followed by the pulse energies given by the kinetic model when experimental data for different fill pressures and output mirror reflectivities are compared to the model's predictions. Furthermore, except at low pressures, there is good agreement with the threshold times given by the model (15 percent difference for the 85 percent output mirror at 11 torr). These disagreements at low pressures with the times to threshold and the lasing times indicate a further physical mechanism is necessary in the kinetic model (perhaps a convection mechanism).

The introduction of a term for the foreign gas into the model suggests that there is an intrinsic amount of impurities in the system. In this case, the gas introduces a further quenching mechanism. In addition, there is a further loss mechanism in the model that accounts for the losses associated with the optical path, possibly aerosol formation which was noted visually at high pressures. After the introduction of these mechanisms into the model, we find the rate coefficients by fitting to the experimental data. Generally, since the trends are followed by the theoretical model, the rate coefficients represent a best value when constrained to be within the range of known uncertainties. Except for the rate coefficients which would be significant at later lasing times than that considered here, and within the appropriate experimental bounds, physically reasonable estimates for the rate coefficients are found. Depending on physical considerations, this estimate is then used to define an upper or lower bound. This gives a range of values the rate coefficients may take. One bound is given experimentally, the other found by the kinetic model presented here.

REFERENCES

1. Wilson, J.W.; Raju, S.; and Shiu, Y.J.: Solar-Simulator-Pumped Atomic Iodine Laser Kinetics. NASA TP-2182, August 1983.

2. Wilson, J.W.; Lee, Y.; Weaver, W.R.; Humes, D.H.; and Lee J.H.: Threshold Kinetics of a Solar-Simulator-Pumped Iodine Laser. NASA TP-2241, February 1984.

3. Brederlow, G.; Fill, E.; and Witte, K.J.: The High-Power Iodine Laser Springer-Verlag, Berlin 1983.

4. Fuss, W.; and Hohla, K. (D.K. Dreyer and R.E. Beverly III, transl.): Pressure Broadening of the 1.3 μm Iodine Laser Line. Rep. No. IPP IV/67, Max-Plank-Inst. Fur Plasmaphysik (Garching Bei Munchen), Dec. 1974. Also Fuss, W.; and Hohla, K.: Pressure Broadening of the 1,3 μm Iodine Laser Line. Z. Naturforsch., vol. 31a, no. 6, June 1976, pp. 569-577.

5. Stock, L. V.; Wilson, J. W.; and Han, K. S.: Simulation Problem for Solar-Pumped Laser. Annual Meeting of Virginia Academy of Science, May 17, 1985.

TABLE I.- PHOTOABSORPTION PARAMETERS USED (6,000 K LIGHT SOURCE) FOR THE EQUIVALENT POWER OF ONE SOLAR CONSTANT EXPOSURE, 1.4 kW/m^2

Parameter	$n\text{-}C_3F_7I$	$i\text{-}C_3F_7I$	I_2 (ref. 7)
σ_o, cm^2	7.9×10^{-19}	6.2×10^{-19}	9.14×10^{-19}
λ_o, nm	272	275	499
δ_o, nm	12.7	14.5	23.0
Φ_I^*	1.0	1.0	0.51
S, sec^{-1}	3.04×10^{-3}	3.37×10^{-3}	3.38×10^{-2}
f	0.652	0.653	0.673

TABLE II. - MEAN REACTION RATE COEFFICIENTS AND ASSOCIATED UNCERTAINTY FACTORS BASED ON LITERATURE VALUES

[The factor in parentheses gives the uncertainty limits associated with the coefficient.]

Reactants	Products	Reaction rate coefficient, $(cm^3)^n/sec$		
		Symbol	$R = n\text{-}C_3F_7$	$R = i\text{-}C_3F_7$
$R + R$	R_2	K_3	$2.6 \times 10^{-12}(4)^{\pm1}$	$9.0 \times 10^{-13}(3.8)^{\pm1}$
$R + I$	RI	K_2	$2.3 \times 10^{-11}(3.5)^{\pm1}$	$3.9 \times 10^{-11}(4.3)^{\pm1}$
$I + I + RI$	$I_2 + R$	C_2	$8.5 \times 10^{-32}(5.3)^{\pm1}$	$8.3 \times 10^{-32}(5.3)^{\pm1}$
$I + I + I_2$	$I_2 + I_2$	C_4	$3.8 \times 10^{-30}(1.3)^{\pm1}$	$3.8 \times 10^{-30}(1.3)^{\pm1}$
$R + RI$	$R_2 + I$	K_4	3×10^{-16}	3×10^{-16}
$R + I^*$	RI	K_1	$5.6 \times 10^{-13}(6.2)^{\pm1}$	$1.7 \times 10^{-13}(17)^{\pm1}$
$I^* + RI$	$I + RI$	Q_1	$2.0 \times 10^{-16}(4.2)^{\pm1}$	$7 \times 10^{-17}(4.1)^{\pm1}$
$I^* + I_2$	$I + I_2$	Q_2	$1.9 \times 10^{-11}(2.6)^{\pm1}$	$1.9 \times 10^{-11}(2.6)^{\pm1}$
$I^* + I + RI$	$I_2 + RI$	C_1	$3.2 \times 10^{-33}(3.2)^{\pm1}$	$3.2 \times 10^{-33}(3.2)^{\pm1}$
$I^* + I + I_2$	$I_2 + I_2$	C_3	$8 \times 10^{-32}(1.8)^{\pm1}$	$8 \times 10^{-32}(1.8)^{\pm1}$
$R + RI$	$R_2 + I^*$	K_5	$3.2 \times 10^{-17}(3.2)^{\pm1}$	$3.2 \times 10^{17}(3.2)^{\pm1}$
$I^* + RI$	RI_2^*	K_6	$8.3 \times 10^{-18}(1.3)^{\pm1}$	$6.5 \times 10^{-18}(1.1)^{\pm1}$

TABLE III.- REACTION RATE COEFFICIENTS FOUND BY NUMERICAL METHODS AND USED IN LASER MODEL

Reaction rate coefficient, $(cm^3)^n/sec$	
Symbol	R = 1-C_3F_7
K_3	9.0×10^{-13}
K_2	$3.9 \times 10^{-11}(4.3)^{0.84}$
C_2	$8.3 \times 10^{-32}(5.3)^{-0.99}$
C_4	3.8×10^{-30}
K_4	3×10^{-16}
K_1	$1.7 \times 10^{-13}(17)^{-0.85}$
Q_1	$7.0 \times 10^{-17}(4.1)^{-0.54}$
Q_2	$1.9 \times 10^{-11}(2.6)^{-0.97}$
C_1	$3.2 \times 10^{-33}(3.2)^{-0.88}$
C_3	8.0×10^{-32}

TABLE IV.- BOUNDS FOR THE REACTION RATE COEFFICIENTS DEFINED BY THIS EXPERIMENT COMPARED TO PREVIOUSLY PUBLISHED RESULTS (ref. 2)

Bound defined by this experiment	Rate coefficient	Bound for previously published results
$1.7 \times 10^{-13}(17)^{-0.85}$	$\geq K_1$ $cm^3/s \geq$	$1.7 \times 10^{-13}(17)^{-1.0}$
$7.0 \times 10^{-17}(4.1)^{-.54}$	$\geq Q_1$ $cm^3/s \geq$	$7.0 \times 10^{-17}(4.1)^{-1.0}$
$3.9 \times 10^{-11}(4.3)^{0.84}$	$\leq K_2$ $cm^3/s \leq$	$3.9 \times 10^{-11}(4.3)^{1.0}$
$1.9 \times 10^{-11}(2.6)^{-0.97}$	$\geq Q_2$ $cm^3/s \geq$	$1.9 \times 10^{-11}(2.6)^{-1.0}$
$8.3 \times 10^{-32}(5.3)^{-0.99}$	$\geq C_2$ $cm^6/s \geq$	$8.3 \times 10^{-32}(5.3)^{-1.0}$

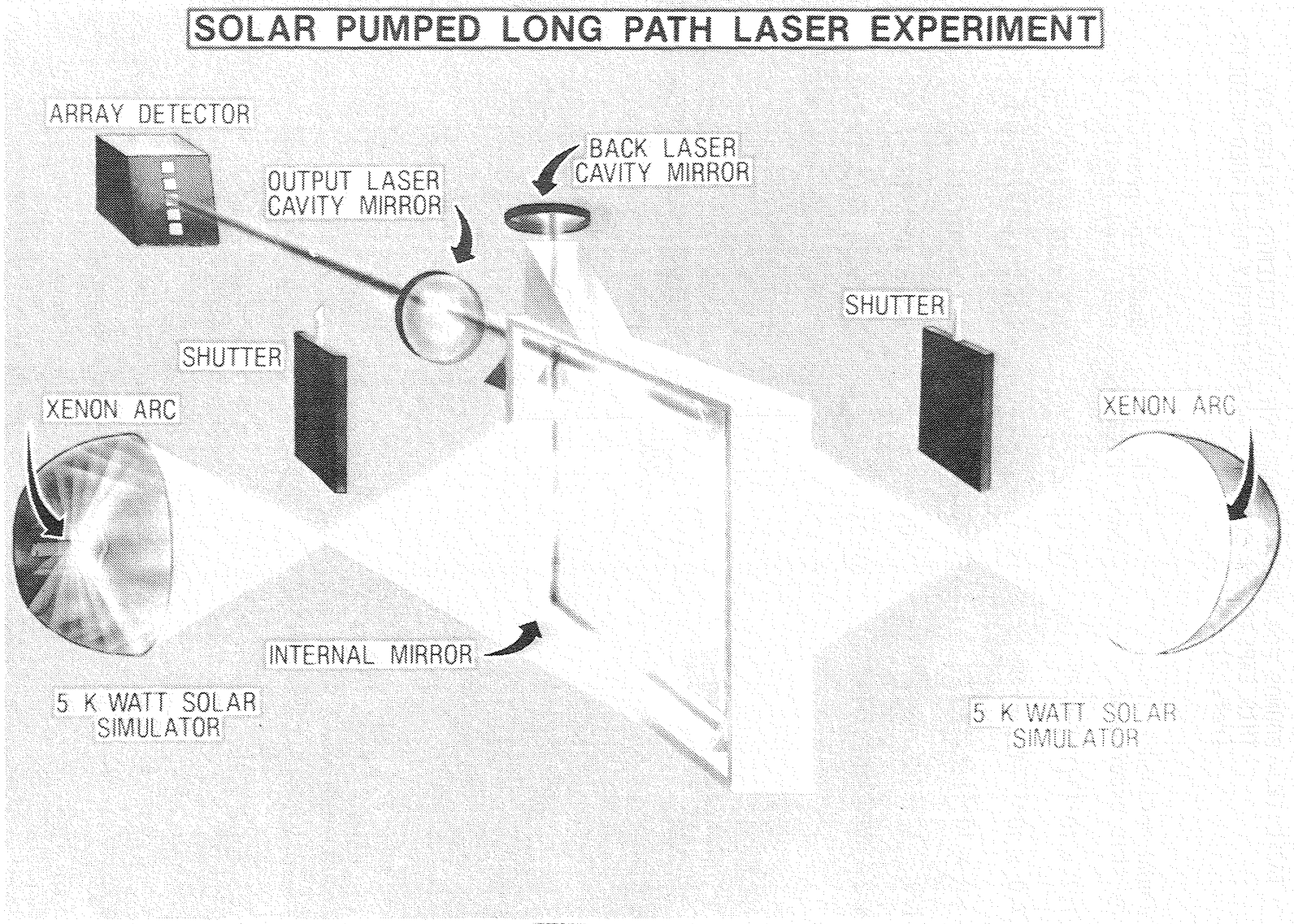

Figure 1.- Solar-pumped long path length laser experiment.

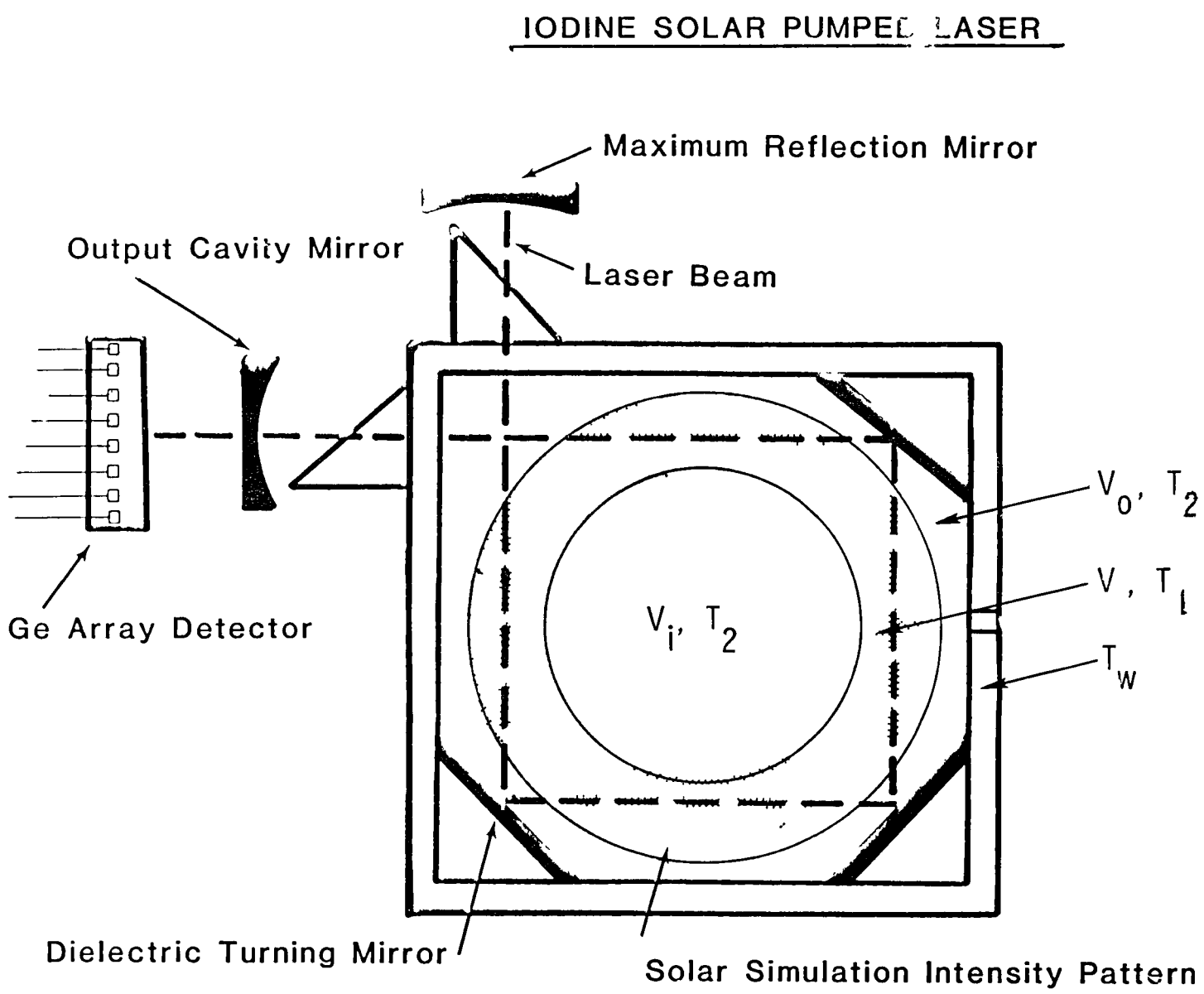

Figure 2.- Temperatures and volumes used to model pressure changes within the active region of the laser cavity.

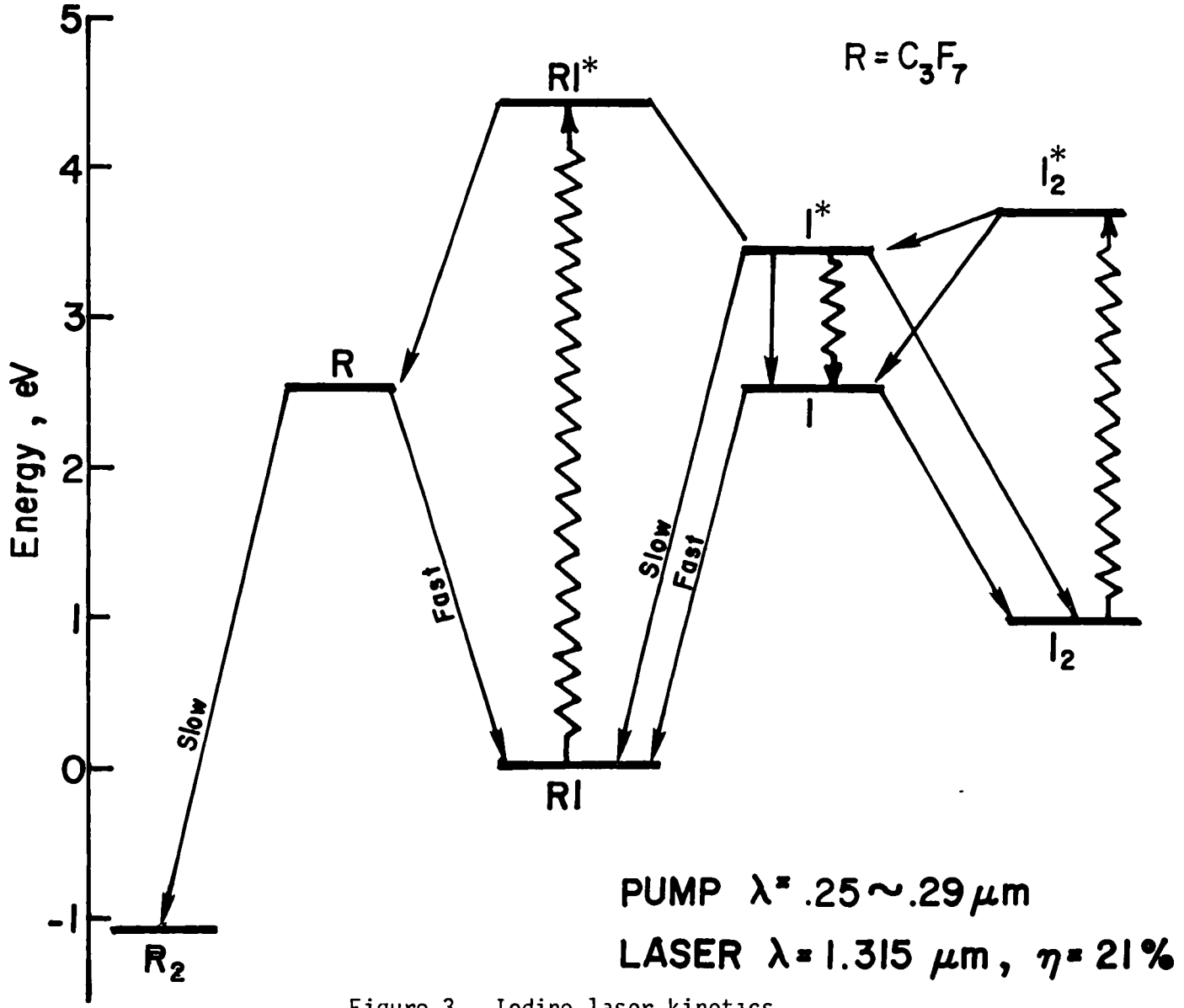

Figure 3.- Iodine laser kinetics.

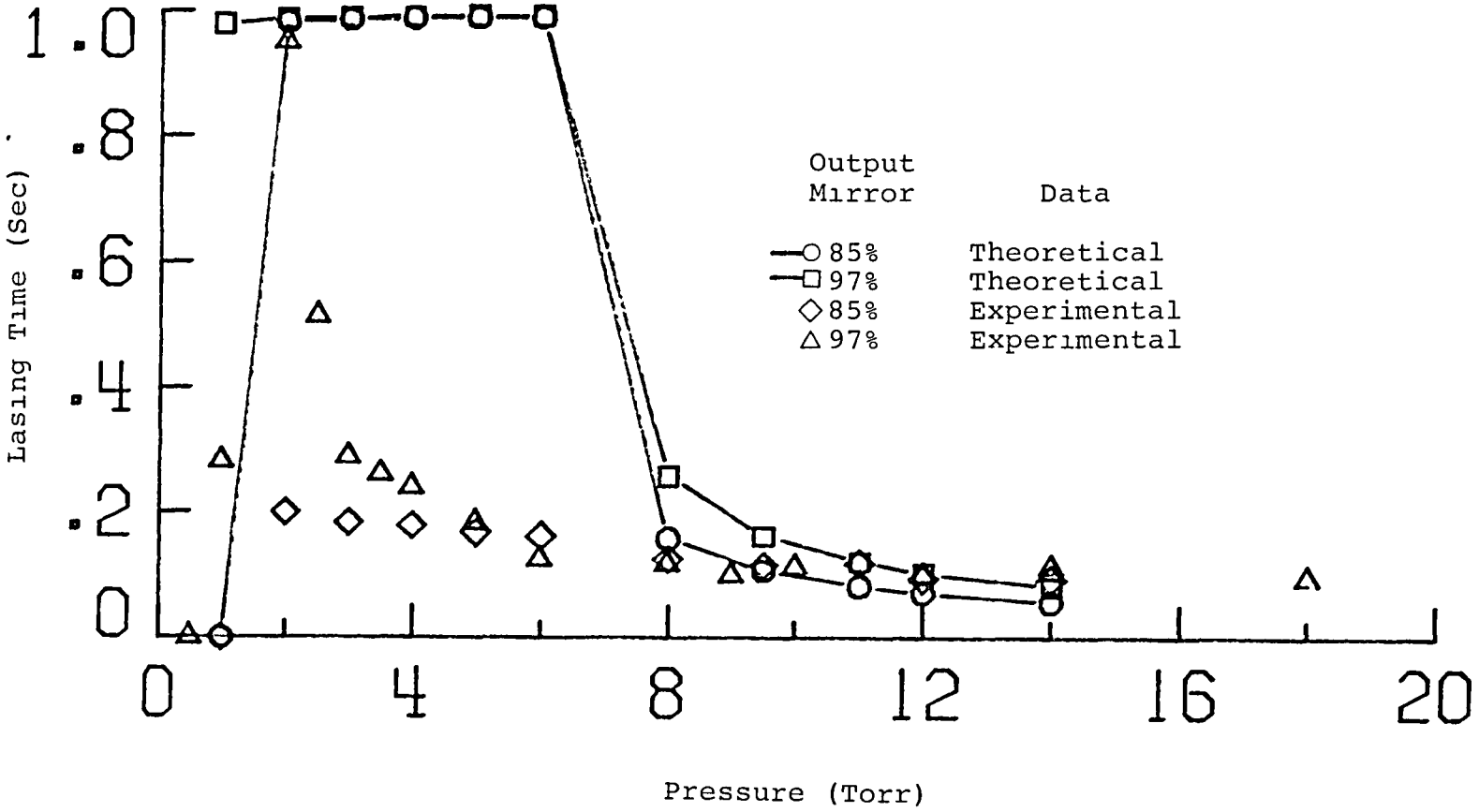

Figure 4.- Results of kinetic model using rate coefficients given in table III for lasing times vs pressure for 85 percent and 97 percent reflectivities as compared to experimental data.

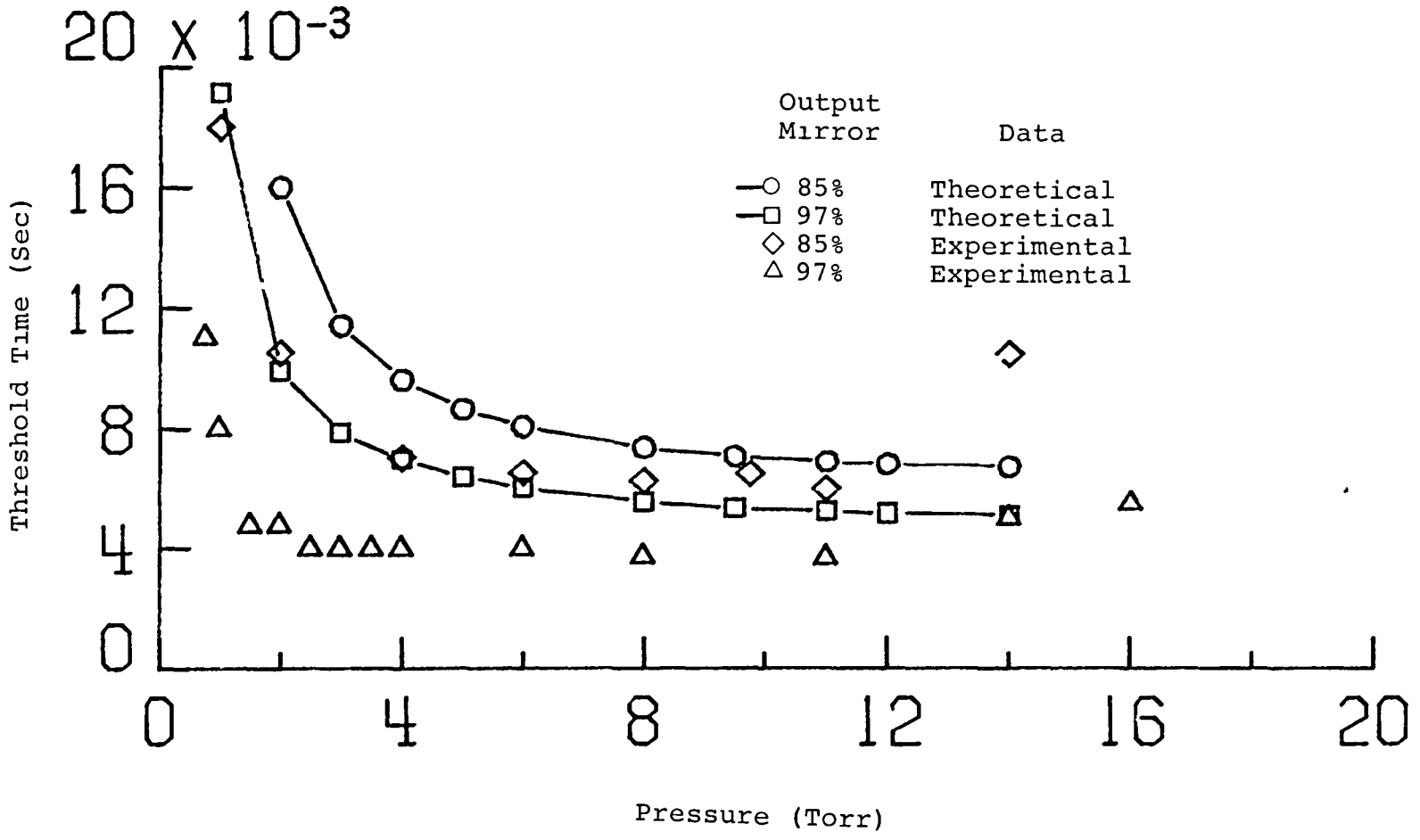

Figure 5.- Results of kinetic model using rate coefficients given in table III for threshold times vs pressure for 85 percent and 97 percent reflectivities as compared to experimental data.

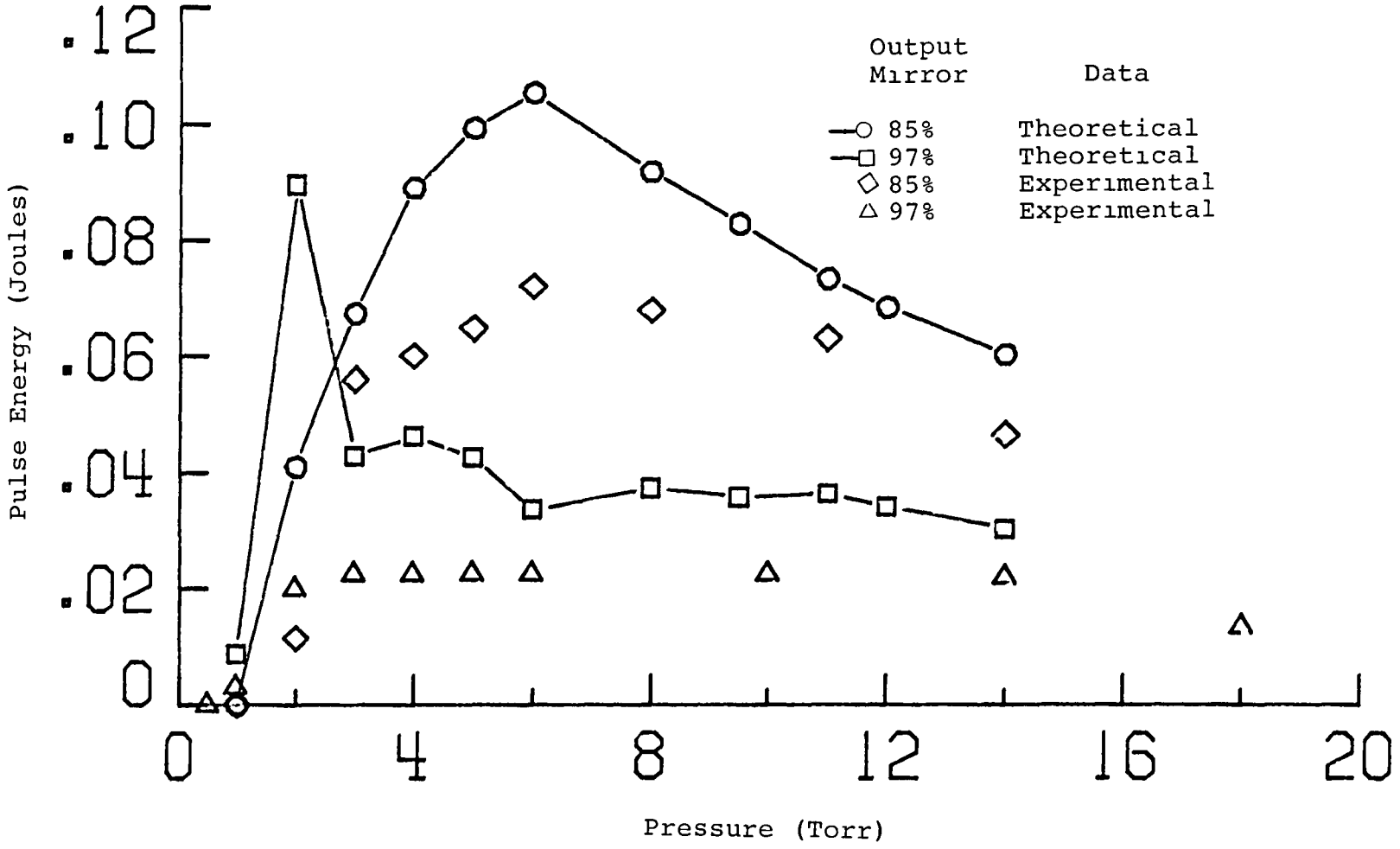

Figure 6.- Results of kinetic model using rate coefficients given in table III and cut-off times given by experiment for pulse energy vs pressure for 85 percent and 97 percent reflectivities as compared to experimental data.

Standard Bibliographic Page

1 Report No	2 Government Accession No	3 Recipient's Catalog No
NASA TM-87668		

4 Title and Subtitle	5 Report Date
A MODEL FOR THE KINETICS OF A SOLAR-PUMPED LONG PATH LASER EXPERIMENT	May 1986
	6 Performing Organization Code: 506-41-41-01
7 Author(s): Larry V. Stock, John W. Wilson and Russell J. De Young	8 Performing Organization Report No
9 Performing Organization Name and Address: Langley Research Center, Hampton, Virginia 23665-5225	10 Work Unit No
	11 Contract or Grant No
12 Sponsoring Agency Name and Address: National Aeronautics and Space Administration, Washington, DC 20546-0001	13 Type of Report and Period Covered: Technical Memorandum
	14 Sponsoring Agency Code

15 Supplementary Notes

Larry V. Stock: Hampton University, Hampton, Virginia. Work performed under NASA Grant NAG-1-411.

John W. Wilson, and Russell J. De Young: Langley Research Center, Hampton, Virginia.

16 Abstract

A kinetic model for a solar-simulator-pumped iodine laser system is developed and compared to an experiment in which the solar simulator output is dispersed over a large active volume (150 cm^3) with low simulator light intensity (≈200 solar constants). A trace foreign gas which quenches the upper level is introduced into the model. Furthermore, a constant representing optical absorption of the stimulated emission is introduced, in addition to a constant representing the scattering at each of the mirrors, via the optical cavity time constant. The non-uniform heating of the gas is treated as well as the pressure change as a function of time within the cavity. With these new phenomena introduced into the kinetic model, a best reasonable fit to the experimental data is found by adjusting the reaction rate coefficients within the range of known uncertainty by numerical methods giving a new bound within this range of uncertainty. The experimental parameters modeled are the lasing time, laser pulse energy, and time to laser threshold.

17 Key Words (Suggested by Authors(s))	18 Distribution Statement
Space Power; Lasers; Solar Laser; Solar Simulator; Photo Chemical	UNCLASSIFIED - Unlimited Subject Category - 36

19 Security Classif (of this report)	20 Security Classif (of this page)	21 No of Pages	22 Price
UNCLASSIFIED	UNCLASSIFIED	34	A03

For sale by the National Technical Information Service, Springfield, Virginia 22161

NASA Langley Form 63 (June 1985)

End of Document